J Solid State Electrochem (2008) 12:1523–1540
DOI 10.1007/s10008-008-0541-3

REVIEW PAPER

Recent advances in synthesis and analysis of Fe(VI) cathodes: solution phase and solid-state Fe(VI) syntheses, reversible thin-film Fe(VI) synthesis, coating-stabilized Fe(VI) synthesis, and Fe(VI) analytical methodologies

Xingwen Yu · Stuart Licht

Received: 18 October 2007 / Accepted: 28 February 2008 / Published online: 2 April 2008

Abstract Fe(VI) batteries based on unusual ferrate cathodic charge storage have been studied for quite a few years. So far, a class of Fe(VI) compounds have been successfully synthesized and studied as the cathodic materials in both alkaline and nonaqueous battery systems. This paper provides a summary of the syntheses of a range of Fe(VI) cathodes including the alkali Fe(VI) salts Li_2FeO_4, $K_xNa_{(2-x)}FeO_4$, K_2FeO_4, Rb_2FeO_4, Cs_2FeO_4, as well as alkali earth Fe(VI) salts $CaFeO_4$, $SrFeO_4$, $BaFeO_4$, and a transition metal Fe(VI) salt Ag_2FeO_4. Two synthesis routes summarized in this paper are the solution phase synthesis and the solid-state synthesis. Preparation of coating-stabilized (coated with $KMnO_4$, SiO_2, TiO_2, or ZrO_2) Fe(VI) cathodes and preparation of thin-film reversible Fe(VI/III) cathodes are also presented. Fe(VI) analytical methodologies summarized in this paper include Fourier transform infrared spectrometry, titrimetric (chromite), ultraviolet-visible spectroscopy, X-ray diffraction, inductively coupled plasma spectroscopy, Mössbauer spectrometry, potentiometric, galvanostatic, and cyclic voltammetry. Cathodic charge transfer of Fe(VI) is also briefly presented.

Keywords Fe(VI) cathode · Synthesis and analysis · Coating stabilization · Reversible thin film

X. Yu (✉)
Department of Chemical and Biological Engineering,
The University of British Columbia,
2360 East Mall,
Vancouver, BC, Canada V6T 1Z3
e-mail: xingwenyu@yahoo.com

S. Licht
Department of Chemistry, University of Massachusetts,
Boston, MA 02125, USA

Introduction

Although hexavalent iron species have been known for over a century, the fascinating chemistry of Fe(VI) is not as established as that for ferrous, Fe(II), ferric, Fe(III), or zero valent (metallic) iron chemistry. As a strong oxidant, Fe (VI), formed in aqueous solutions as FeO_4^{2-}, has been investigated for several decades as a potentially less hazardous alternative to the chlorination purification of water [1–5] and as the catalysts in organic synthesis [6]. The field of solid Fe(VI) compounds for charge storage was introduced in 1999, and at that time the term "super-iron" was coined to refer to the class of materials which contain "super-oxidized" iron in the unusual hexavalent state [7]. The charge transfer chemistry of Fe(VI) salts in both aqueous and nonaqueous media has been probed [7–47].

So far, a class of Fe(VI) compounds have been successfully synthesized and studied as the cathodic materials in battery systems. In conventional syntheses, high purity K_2FeO_4 is generally prepared from alkaline hypochlorite oxidation of Fe(III) [6, 48]. Recently, this conventional synthesis methodology was further developed by a few research groups [13, 32, 49–51]. The less soluble Fe(VI) salts can be prepared by precipitation upon addition of various salts to solutions containing dissolved FeO_4^{2-} [13, 14]. More recently, other two novel Fe(VI) synthesis routs have also been successfully developed, including the solid phase Fe(VI) synthesis [21] and direct electrochemical Fe(VI) synthesis [20, 25, 27, 28, 52–56]. This paper provides a review of the recent advances in the solution phase Fe(VI) synthesis and solid-state Fe(VI) synthesis, including a brief summary of K_2FeO_4 synthesis by the solution phase oxidation of Fe(III) developed from the conventional method, the syntheses of less soluble Fe(VI) salts by dissolution of FeO_4^{2-} and precipitation with

alternate cations, and the solid-state Fe(VI) synthesis route which uses only solid-state reactants. Fe(VI) salts with synthetic details summarized in this paper include the alkali Fe(VI) salts Li_2FeO_4, $K_xNa_{(2-x)}FeO_4$, Rb_2FeO_4, Cs_2FeO_4, as well as alkali earth Fe(VI) salts $CaFeO_4$, $SrFeO_4$, $BaFeO_4$, and a transition metal Fe(VI) salt Ag_2FeO_4.

Cathodic charge transfer of the synthesized Fe(VI) salts is briefly presented in this paper. Fe(VI) sustains high capacity 3-electron charge transfer. However, most of Fe(VI) cathodes tend to be passivated in alkaline battery systems upon storage. This paper also summarizes preparation details of K_2MnO_4-, TiO_2-, SiO_2-, and ZrO_2-coated Fe(VI) cathodes. With these coatings, robustness and stability of Fe(VI) cathodes are greatly improved. Preparation details of reversible Fe(VI/III) thin film towards a rechargeable Fe (VI) cathode is also presented in this paper. Finally, various Fe(VI) analytical methodologies are summarized, which include FTIR (Fourier transform infrared) spectrometry, titrimetric (chromite), UV/Vis (ultraviolet-visible) spectroscopy, XRD (X-ray diffraction), ICP (inductively coupled plasma) spectroscopy, Mössbauer spectrometry, potentiometric, galvanostatic, and cyclic voltammetry.

Solution phase syntheses of K_2FeO_4, $K_xNa_{(2-x)}FeO_4$, Cs_2FeO_4, Rb_2FeO_4, Li_2FeO_4, $SrFeO_4$, $BaFeO_4$, $CaFeO_4$ and Ag_2FeO_4

So far, a class of Fe(VI) cathodes including Li_2FeO_4, $K_xNa_{(2-x)}FeO_4$, K_2FeO_4, Rb_2FeO_4, Cs_2FeO_4, $CaFeO_4$, $SrFeO_4$, $BaFeO_4$, and Ag_2FeO_4 have been successfully synthesized. Among these Fe(VI) compounds, K_2FeO_4 is readily synthesized and usually used as the precursor for other Fe(VI) syntheses. In this section, synthesis of K_2FeO_4 is first briefly introduced. Then, solution phase syntheses of other Fe(VI) cathodes with K_2FeO_4 as the precursor are summarized.

In recent Fe(VI) charge transfer studies, solid K_2FeO_4 was generally synthesized by the chemical solution phase oxidation of Fe(III) to Fe(VI) in the alkaline medium [13, 32, 40, 49–51] developed from a conventional synthesis methodology [6, 48]. This wet chemical synthesis route is complex and includes a key step of oxidation of Fe(III) to Fe(VI) by hypochlorite. With this synthesis route, Licht et al. illustrated a synthesis yielding 80~100 g 96.5% to 99.5% pure K_2FeO_4, and the product of this synthesis is demonstrated to have a lifetime on the order of years [13]. Walz et al. demonstrated a batch synthesis that generated 30~40 g of solid K_2FeO_4, at 40–50% experimental yield [32, 40]. Li et al. improved some procedures of this synthesis method and obtained the high purity K_2FeO_4 [49]. However, this complex wet chemical synthesis can be a challenge: for example, small variations in the filtration, purification, and drying processes can lead to decomposition and diminish purities.

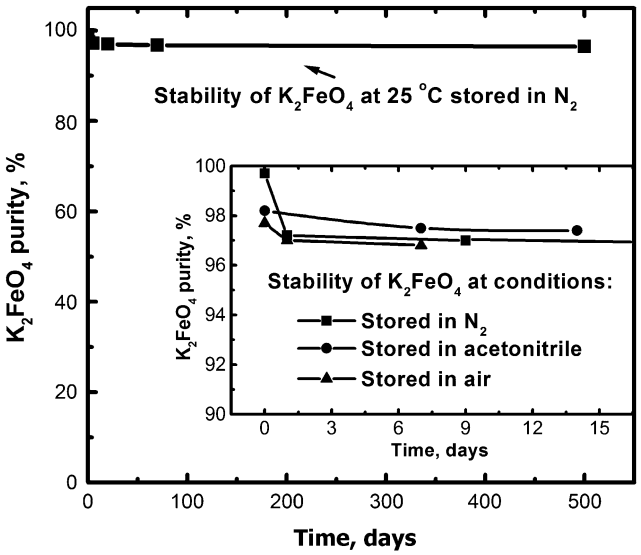

Fig. 1 The long-term stability of K_2FeO_4 measured after sealing in a variety of conditions [13]

The percentage of iron can be determined by ICP (inductively coupled plasma) spectroscopy, and the percentage the original iron containing material which is converted to solid Fe(VI) salt may be determined by UV/Vis spectroscopy and by the chromite method. These analyses methodologies will be presented in the later section of this review. K_2FeO_4, prepared with the solution phase synthesis, is particularly robust. A long-term stability (over 1 year) of K_2FeO_4 is presented in the main portion of Fig. 1. K_2FeO_4 appears to be stable whether sealed under dry N_2 or sealed in air and is also stable under acetonitrile (Fig. 1 inset) [13].

With K_2FeO_4 as the precursor, recently, alkali Fe(VI) salts Li_2FeO_4, Na(K)FeO_4, Rb(K)FeO_4, and Cs_2FeO_4 have been successfully synthesized by dissolution of FeO_4^{2-} and precipitation with alternate cations (Li^+, Na^+, Rb^+, Cs^+) [11, 30]. The Na(K)FeO_4, Rb(K)FeO_4, and Cs_2FeO_4 salts can be synthesized from K_2FeO_4 by driving formation via their hydroxide reaction, in the respective Na, Cs, or Rb hydroxide solution [30]. In these media, Fe(VI) Na, Cs, or Rb salts can be obtained from the full (Eq. 1) or partial (Eq. 2) replacement precipitation reactions:

$$K_2FeO_{4-aq} + 2MOH_{aq} \rightarrow M_2FeO_{4-solid} + 2KOH_{-aq}; \quad M = Na, Cs \text{ or } Rb \tag{1}$$

$$K_2FeO_{4-aq} + xMOH_{aq} \rightarrow M_xK_{(2-x)}FeO_{4-solid} + xKOH_{-aq}; \quad M = Na, Cs \text{ or } Rb \tag{2}$$

In these syntheses, Licht et al. [30] proved that the conversion from the K_2FeO_4 to Cs_2FeO_4 can be complete, and the purity of the resultant Cs_2FeO_4 can be up to 99.2%. In the Rb case, the synthesis can yield of 98.7% purity $Rb_{1.7}K_{0.3}FeO_4$. Synthesis of sodium ferrate by reaction of K_2FeO_4 with Na salts leads to a mixed Na/K salt, as $Na_{1.1}K_{0.9}FeO_4$ with 96.3% purity. Traditionally, the preparation of pure Li_2FeO_4 has been a technical challenge and rarely studied. Licht's group [11] has improved on the synthesis of Gump and Wagner [57] by the addition of a final acetonitrile wash to produce Li_2FeO_4 with higher purity [11].

The main portion of Fig. 2 compares the 71 °C stability of Cs_2FeO_4, K_2FeO_4, $Rb_{1.7}K_{0.3}FeO_4$, and $Na_{1.1}K_{0.9}FeO_4$. It is seen that K_2FeO_4 exhibits the highest stability and that there is a modest trend of a purity drop with time for $Na_{1.1}K_{0.9}FeO_4$, $Rb_{1.7}K_{0.3}FeO_4$, and Cs_2FeO_4. Inset of Fig. 2 compares the solubility of Cs, the mixed Rb, and Na/K Fe(VI) salts in KOH electrolytes. Of interest is the domain of the high concentration KOH electrolytes, which includes the electrolyte used in the conventional alkaline batteries. As seen in the figure, for each of the alkali Fe(VI) salts, soluble Fe(VI) concentration decreases with increasing KOH concentration and solubility is in the millimolar domain in a saturated KOH electrolyte. In addition, the solubility, S, varies in the order of $S(Na_{1.1}K_{0.9}FeO_4) > S(K_2FeO_4) > S(Rb_{1.7}K_{0.3}FeO_4) > S(Cs_2FeO_4)$ [30].

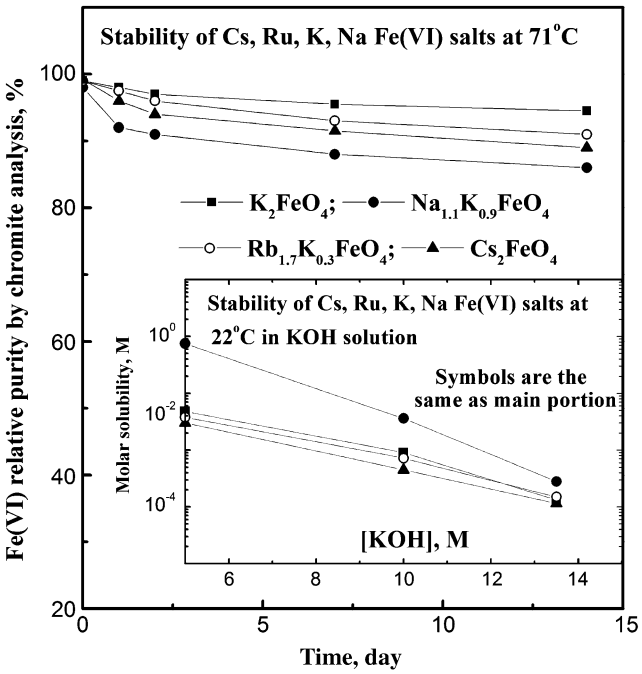

Fig. 2 Solid-state stability of Cs_2FeO_4, K_2FeO_4, $Rb_{1.7}K_{0.3}FeO_4$, and $Na_{1.1}K_{0.9}FeO_4$ at 71 °C. Inset: Room temperature solubility of Cs_2FeO_4, K_2FeO_4, $Rb_{1.7}K_{0.3}FeO_4$, and $Na_{1.1}K_{0.9}FeO_4$ in various hydroxide solutions [30]

As the synthesis of alkali Fe(VI) salts, the dried K_2FeO_4 may be used for alkaline earth Fe(VI) salts $BaFeO_4$, $SrFeO_4$, and $CaFeO_4$ syntheses [12, 13, 32, 40, 46, 47, 58–60]. The salts are synthesized by utilizing the higher alkaline insolubility of Sr, Ca, or Ba Fe(VI) compared to that of K_2FeO_4. $BaFeO_4$ may be synthesized from barium hydroxide based on the reaction described as Eq. 3. $BaFeO_4$ and $SrFeO_4$ may also be synthesized from the respective acetate salts in accord with the reaction Eq. 4 [12, 13, 32, 40, 46, 58–60].

$$K_2FeO_{4-aq} + Ba(OH)_{2-aq} \rightarrow BaFeO_{4-solid} + 2KOH \quad (3)$$

$$K_2FeO_{4-aq} + M(C_2H_3O_2)_{2-aq} \rightarrow MFeO_{4-solid} + KC_2H_3O_{2-aq}; \quad (4)$$

$$M = Sr \text{ or } Ba$$

Figure 3 compares the solubilities of Sr, K, and Ba Fe (VI) salts in the alkaline electrolytes. At all concentrations through KOH saturation, $SrFeO_4$ is more soluble than the minimum case of $BaFeO_4$'s solubility in a $KOH/Ba(OH)_2$ electrolyte. Furthermore, at low KOH concentrations, $SrFeO_4$ is more soluble than K_2FeO_4. However, of significance is the domain of the most concentrated KOH electrolytes, which includes the electrolyte used in conventional alkaline batteries [12].

Recently, Xu et al. [47] successfully synthesized $CaFeO_4$ from K_2FeO_4, with $Ca(NO_3)_2$ and $Ca(OH)_2$ as the precursors. This synthesis overcame the drawback of the earlier $CaFeO_4$ synthesis by exchange reactions between $BaFeO_4$ and K_2FeO_4, which have been difficult to

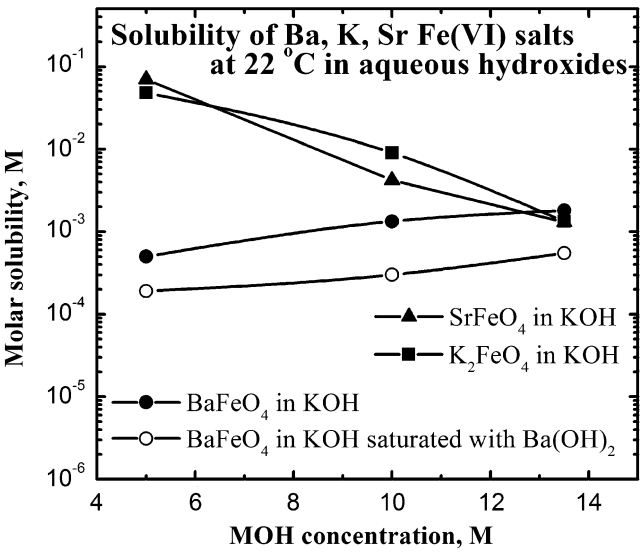

Fig. 3 Room temperature solubility of $BaFeO_4$, K_2FeO_4, and $SrFeO_4$ in various aqueous hydroxide electrolytes [12]

reproduce [61, 62]. Xu et al. also studied the stability of the synthesized $CaFeO_4$. Figure 4 shows the stability of $CaFeO_4$ samples with various purities at different temperatures. The purity of $CaFeO_4$ decreases with the prolongation of conserved time at all the temperatures, and the decomposition rate increases with the increase of temperature. Xu et al. proposed that the poor stability of $CaFeO_4$ might be due to its relatively higher Fe(III) impurity, crystalloid and/or absorbent water, and the stronger polarization effect of Ca^{2+} ion on FeO_4^{2-} [47, 63].

Ag_2FeO_4 has been firstly synthesized and investigated as a selective oxidation agent for organic synthesis. However, the synthesized Ag_2FeO_4 was only moderately stable [64]. Licht et al. recently investigated the use of Ag_2FeO_4 as a cathode material for batteries and reported that the silver Fe (VI) compounds could be chemically synthesized by conversion from K_2FeO_4 or $BaFeO_4$ via substitution reaction with $AgNO_3$ (Eq. 5). However, the best results were obtained when K_2FeO_4 was used as the precursor [33]:

$$K_2FeO_4 + 2AgNO_3 \rightarrow Ag_2FeO_4 + 2KNO_3 \quad (5)$$

The stability of Ag_2FeO_4 is considerably less, and only when stored in the freezer (at 0 °C) is the material moderately stable over a period of 1 week (Fig. 5). At higher temperatures, the Ag_2FeO_4 purity falls more rapidly [33].

FTIR spectrometry is an effective technique for the Fe (VI) salts characterization and has been commonly used for characterization of the synthesized Fe(VI) cathodes by different research groups. Licht et al. compared the FTIR spectra for the synthesized a K_2FeO_4, Cs_2FeO_4, Ru(K) FeO_4, $BaFeO_4$, and $SrFeO_4$ (Fig. 6) [30]. The Cs_2FeO_4 compared to K_2FeO_4 spectra are similar, with the principal difference between these two in the 798 compared to 807 cm^{-1} absorption peak for the Cs_2FeO_4 compared to

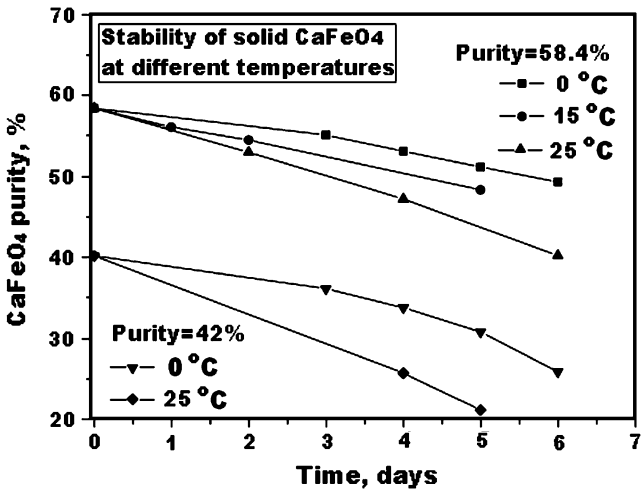

Fig. 4 Stability of solid $CaFeO_4$ with various purities at different temperatures. Purity of $CaFeO_4$ is determined by chromite analysis [47]

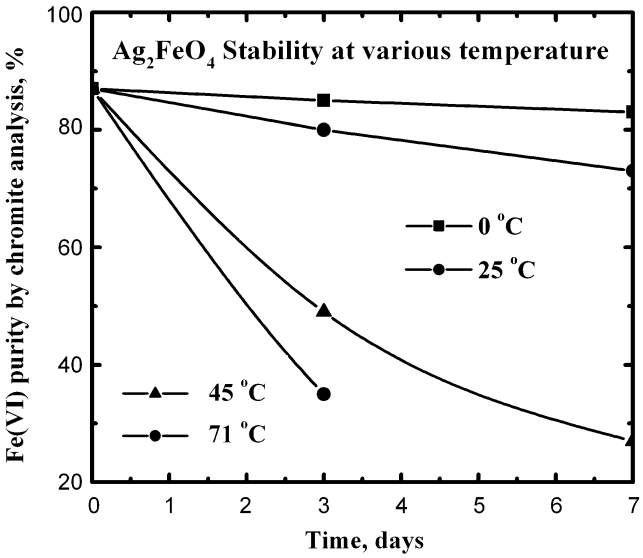

Fig. 5 Solid-state stability of Ag_2FeO_4 at 0, 25, 45, and 71 °C [33]

K_2FeO_4 compound. Unlike the Cs salt, conversion to Rb from K was generally incomplete as described in previous section. FTIR spectrum of the mixed Rb/K Fe(VI) salt synthesized by Licht et al. results in IR (infrared) absorption peaks which are largely indistinguishable from the pure K_2FeO_4. As seen in Fig. 6, the spectrum appearance is intermediate to that observed for either the pure K_2FeO_4 or Cs_2FeO_4. The location and magnitude of these near lying Fe(VI) absorption peaks differ from the spectra of the lower valence Fe state salts including Fe_3O_4, Fe_2O_3, or $Fe(OH)_3$ [65, 66]. In the pure potassium salt case, the IR stretching frequencies of K_2FeO_4 had been interpreted as evidence of the equivalence, symmetric, and tetrahedral distribution of the oxygen atoms surrounding the iron center [67]. For the incompletely converted sodium Fe(VI) salt $Na_{1.1}K_{0.9}FeO_4$ synthesized by Licht et al., as shown in Fig. 7, the $Na_{1.1}K_{0.9}FeO_4$ appears to act as a mixture of 55 equivalent percent Na_2FeO_4 and 45% K_2FeO_4. The spectra of $BaFeO_4$ and $SrFeO_4$ are readily distinguishable and are consistent with the early IR and FTIR qualitative determination of the $BaFeO_4$ [67]. However, the $SrFeO_4$ spectrum is more complex than observed for either K_2FeO_4 or $BaFeO_4$. The observed IR spectrum of Ag_2FeO_4 is not similar to other Fe(VI) compounds. Figure 8 compares the FTIR spectra of Ag_2FeO_4 with the Ag_2O and the K_2FeO_4 [33]. In this figure, the Ag_2FeO_4 compound does not display the significant IR Fe(VI) absorption peaks in the 750 to 850 cm^{-1} range. Xu et al. first reported the FTIR analysis of calcium ferrate(VI), which is displayed as Fig. 9. The characteristic peaks of $CaFeO_4$ have similar shapes with those of $BaFeO_4$, albeit the positions and relative intensities of the peaks are a little different [47].

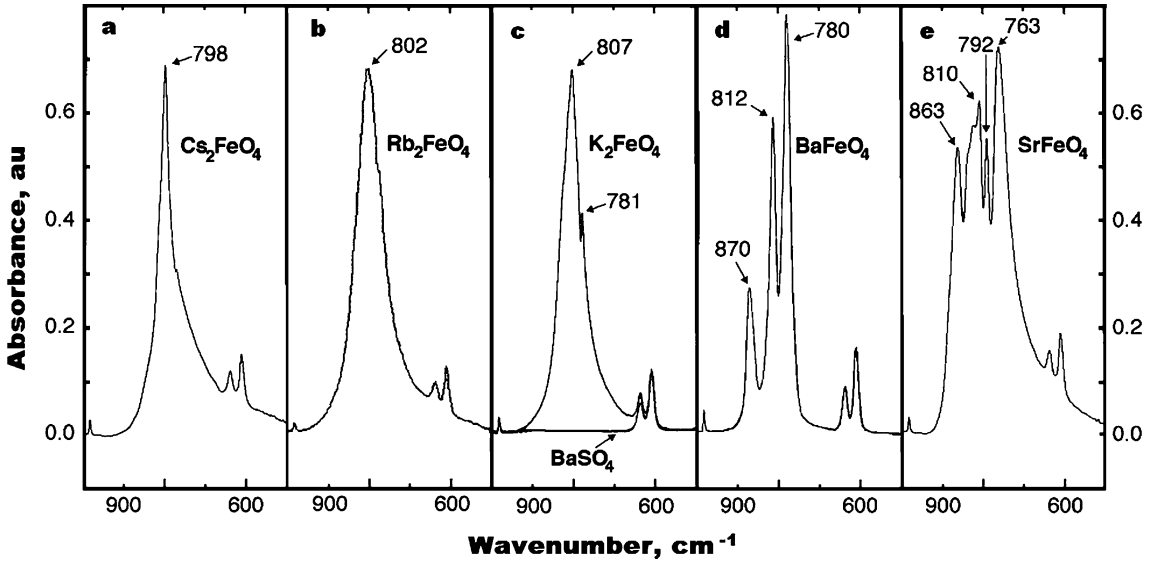

Fig. 6 FTIR absorption of solid alkali ferrates K_2FeO_4, $Ru_{1.7}K_{0.3}FeO_4$, and Cs_2FeO_4, and alkali earth ferrates $BaFeO_4$ and $SrFeO_4$. Spectra were measured with a Vector 22 BRUKER FTIR in a conventional KBr pellet [30]

Solid synthesis of $BaFeO_4$

Solid phase reaction preparation of $BaFeO_4$ was developed by Licht et al. Specially, in this synthesis [21], the $BaFeO_4$ was obtained by grinding the mix of 1 equivalent of solid K_2FeO_4, 0.5 equivalent of solid $Ba(OH)_2{\cdot}8H_2O$ and 0.5 equivalent of solid BaO. With this synthesis route, Licht et al. obtained 97% $BaFeO_4$ [21]. Actually, optimizing the solid phase $BaFeO_4$ synthesis has been accomplished in quite a few steps [21]. Licht et al. found that there is no room temperature reaction for a 1:1 mole ratio of solid BaO to solid K_2FeO_4. However, conversion to $BaFeO_4$ can be achieved by replacing the BaO with solid $Ba(OH)_2{\cdot}8H_2O$. This is due to the presence of bound water, included within the hydrated solid $Ba(OH)_2$ salt, which can facilitate the conversion reaction to yield $BaFeO_4$.

The use of solid-state reactants has several Fe(VI) synthetic advantages. Fe(VI) solution phase degradation to Fe(III) is avoided, and fewer preparatory steps reduce requisite synthesis time and can increase the yield of the Fe (VI) salt synthesis. For example, in the solution phase synthesis of $BaFeO_4$, both K_2FeO_4 and $Ba(OH)_2$ are reacted in the aqueous phase, and $BaFeO_4$ is generated due to the higher alkaline insolubility of barium ferrate(VI) compared to that of potassium ferrate(VI) [13]. In the solid synthesis, the reactants such as K_2FeO_4 and barium oxide

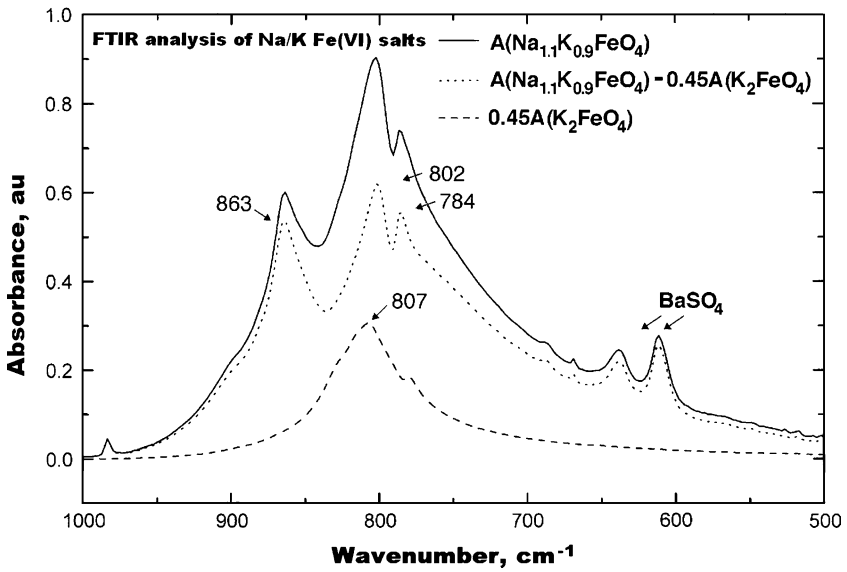

Fig. 7 FTIR absorption of solid $Na_{1.1}K_{0.9}FeO_4$ and K_2FeO_4, as well as the computed spectra of pure Na_2FeO_4 (by deconvolution of these spectra). Spectra were measured with a Vector 22 BRUKER FTIR in a conventional KBr pellet [30]

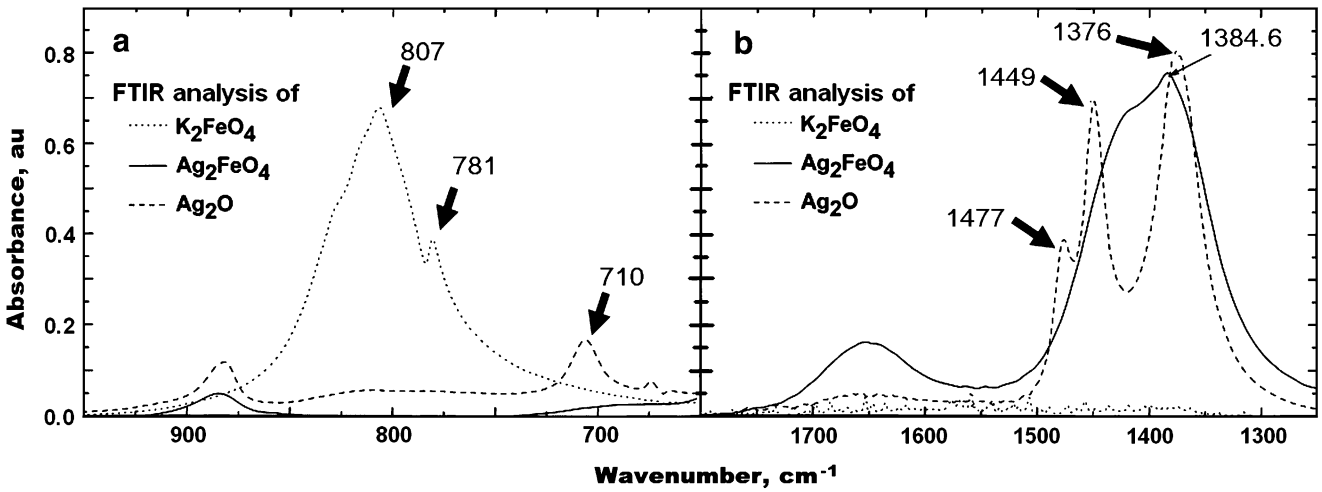

Fig. 8 FTIR absorption of solid Ag_2FeO_4, Ag_2O, and K_2FeO_4. Spectra were measured with a Vector 22 BRUKER FTIR in a conventional KBr pellet [33]

alone are stable, but fully react upon grinding together, forming a dough-like paste; KOH is removed, isolating the Fe(VI) salt. In the barium example, water, bound in the salt as the hydrate $BaO{\cdot}4H_2O$ is necessary to drive the reaction, but minimizes water in the synthesis and forms an unusually pure (>98%) and more stable (compared to solution phase synthesized $BaFeO_4$) Fe(VI) salt (as illustrated in Fig. 10) [21].

Cathodic charge transfer of synthesized Fe(VI) salts

The use of Fe(VI) salts as alkaline cathodic charge storage materials is based on the energetic and high-capacity $3e^-$ reduction of Fe(VI) to a ferric oxide or hydroxide product. In a manner analogous to the alkaline oxidation product of zinc, whose zincate product varies with the discharge and the composition of the electrolyte, the degree of hydration and any associated cation of Fe(VI)'s ferric product will depend on the extent of reduction and the composition of the hydroxide electrolyte. The $3e^-$ cathodic charge storage of Fe(VI) is presented in Eq. 6 or Eq. 7 via the reduction of the alkaline Fe(VI) species, FeO_4^{2-}, respectively, to the ferric hydroxide or anhydrous oxide product [7, 68, 69].

$$FeO_4^{2-} + 3H_2O + 3e^- \rightarrow FeOOH + 5OH^- \quad (6)$$

$$FeO_4^{2-} + 5/2H_2O + 3e^- \rightarrow 1/2Fe_2O_3 + 5OH^- \quad (7)$$
$$E = 0.5 - 0.65V \text{ vs. SHE}$$

Various Fe(VI) salts exhibit the typical Fe(VI) alkaline cathodic discharge. The theoretical $3e^-$ charge capacity of the Fe(VI) salts are determined as: 3 $F{\times}MW^{-1}$, from the salt molecular weight, MW(g/mol), and the Faraday constant (F=96,485 coulomb/mol=26,801 mA·h/mol). The theoretical capacities of various Fe(VI) salts are listed in Table 1.

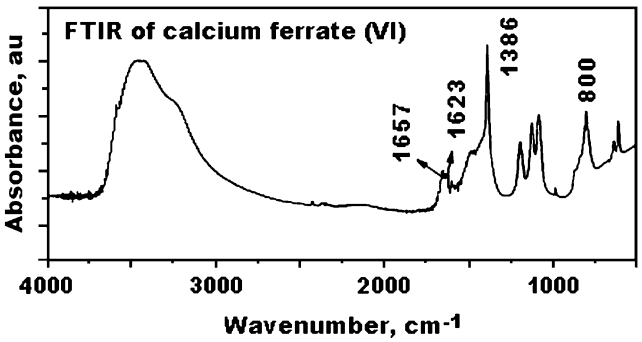

Fig. 9 FTIR spectra for calcium ferrate(VI), $CaFeO_4$. Spectra were measured by a Nicolet Nexus 670 Fourier transform infrared spectrophotometer in a conventional KBr pellet [47]

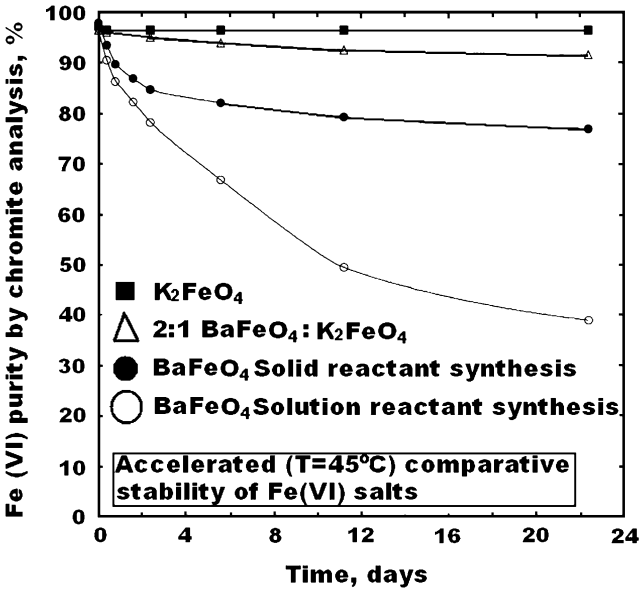

Fig. 10 The 45 °C stability after storage of K_2FeO_4, $BaFeO_4$, and $K_2FeO_4/BaFeO_4$ mixed salts as determined by chromite analysis [21]

Table 1 Theoretical 3-electron charge capacities of various Fe(VI) salts

Fe(VI) salts	Charge storage	Intrinsic capacity (mAh/g)
Li_2FeO_4	$3e^-$	601
Na_2FeO_4	$3e^-$	485
K_2FeO_4	$3e^-$	406
Rb_2FeO_4	$3e^-$	276
Cs_2FeO_4	$3e^-$	209
$SrFeO_4$	$3e^-$	388
$BaFeO_4$	$3e^-$	313
$CaFeO_4$	$3e^-$	502
Ag_2FeO_4	$5e^-$	399

A primary alkaline Fe(VI) battery contains a Fe(VI) cathode and can utilize the zinc anode and alkaline electrolyte from a conventional alkaline battery. In a zinc alkaline battery, the zinc anode generates a distribution of zinc oxide and zincate products and, similarly, the final Fe (VI) product will depend on the depth of discharge. The general discharge of alkaline electrolyte cells utilizing a Zn anode and Fe(VI) cathodes is expressed as:

$$\mathrm{MFeO_4} + 3/2\mathrm{Zn} \rightarrow 1/2\mathrm{Fe_2O_3} + 1/2\mathrm{ZnO} + \mathrm{MZnO_2} \quad \mathrm{M} = \mathrm{Li_2}, \mathrm{Na_2}, \mathrm{K_2}, \mathrm{Ru_2}, \mathrm{Cs_2}, \mathrm{Sr}, \mathrm{Ba}, \mathrm{Ca} \tag{8}$$

Ag_2FeO_4 is of interest, this Fe(VI) salt has an intrinsic cathodic capacity that includes not only the $3e^-$ Fe(VI) reduction, but also the single electron reduction of each of two Ag(I), for at total 5 Faraday per mole or 399.3 mA h/g intrinsic capacity, in accord with Eq. 9 [33].

$$\mathrm{Ag_2FeO_4} + 5/2\mathrm{H_2O} + 5\mathrm{e}^- \rightarrow 2\mathrm{Ag} + 1/2\mathrm{Fe_2O_3} + 5\mathrm{OH}^- \tag{9}$$

Thus, the discharge of alkaline Ag_2FeO_4 cathode, Zn anode Fe(VI) cell, will be expressed as:

$$\mathrm{Ag_2FeO_4} + 5/2\mathrm{Zn} \rightarrow 1/2\mathrm{Fe_2O_3} + 2\mathrm{Ag} + 5/2\mathrm{ZnO} \tag{10}$$

Discharge capacity of K_2FeO_4 and $BaFeO_4$ cathodes is normally higher than that of MnO_2 cathode [7, 68]. The energy capacities of K_2FeO_4, $BaFeO_4$, and conventional MnO_2 cathode, alkaline primary batteries with a Zn anode were compared in Fig. 11. In both the low- (6,000 Ω, current density J=0.25 mA/cm^2) and high- (500 Ω, J= 3 mA/cm^2) discharge domain, the K_2FeO_4 cell generates significantly higher capacity than does the MnO_2 cell. Of the three cells examined, the $BaFeO_4$ cathode cell exhibits the highest coulombic efficiency at high discharge rates (J> 10 mA/cm^2), resulting in the observed higher energy capacity despite the lower intrinsic charge capacity of $BaFeO_4$ compared to K_2FeO_4 [7].

Figure 12 compares the constant load discharge of Fe (VI) batteries containing the Na, K, Rb, Cs, and Ba Fe(VI) cathodes discharged at the same condition [30]. As observed in the figure, the alternate Cs, Rb, and Na mix cathodes discharge to a significant fraction of their respective intrinsic capacities of 209 mA h/g for Cs_2FeO_4, 290 mAh/g for $Rb_{1.7}K_{0.3}FeO_4$, and 445 mAh/g for $Na_{1.1}K_{0.9}FeO_4$. Each of the Fe(VI) cathodes is similar in discharge potential but does not generate quite as a high coulombic efficiency as the $BaFeO_4$ cathode [30].

Figure 13 compares the $SrFeO_4$, K_2FeO_4, and $BaFeO_4$ Fe(VI) batteries under the same constant load discharge condition. Under these conditions, the strontium Fe(VI) cathode discharges to ~1.5 Wh, a significantly higher energy than that generated by the K_2FeO_4 cathode, and approaching that of the $BaFeO_4$ cathode cell. The strontium cathode cells typically exhibit ~20 to 40 mV higher open circuit voltage than the equivalent barium cell, and as seen in the figure, a higher potential average is exhibited when the strontium cell is discharged under low (75 Ω) load [12].

Open circuit voltage (OCV) of Ag_2FeO_4–Zn battery was observed to be 1.86 V. As seen in Fig. 14, for the Ag_2FeO_4 with 10 wt% graphite discharge curve, the coulombic efficiency of the Ag_2FeO_4 salt is less than that for either the K_2FeO_4 or AgO/K_2FeO_4 composite cathodes. However, using 30%, rather than 10%, graphite in the Ag_2FeO_4 cathode mix results in a substantial increase of the Ag_2FeO_4 discharge efficiency, accessing more than 80% of the theoretical $5e^-$ capacity of the Ag_2FeO_4. A two-step potential is observed during the discharge process. Consistent with the three of the five electrons accessed in the process of Fe(VI) reduction, approximately 60% of the discharge occurs at the higher potential. Consistent with two of the five electrons accessed in the process of Ag(I) reduction, approximately 40% of the discharge is observed to occur at the lower potential [33].

Figure 15 compares the discharge curves of $CaFeO_4$ and K_2FeO_4 electrodes at various currents at 15 °C. At lower discharge rate, the $CaFeO_4$ displays smaller discharge capacity than K_2FeO_4. However, at higher discharge rate (discharge current 100 m A/g), $CaFeO_4$ displays not only much higher discharge potential but also much higher discharge capacity than K_2FeO_4 electrode. This indicates that $CaFeO_4$, somehow like $BaFeO_4$, has the better intrinsic rate discharge capability [47].

The attempt of using Fe(VI) salts as the cathode in nonaqueous battery has also been reported [11, 70]. The discharge of Fe(VI) in nonaqueous Fe(VI) battery is complicated. Licht's group proposed that a Fe(VI) storage mechanism in Li containing nonaqueous media was through the insertion of Li^+ [11]:

$$\mathrm{MFeO_4} + x\mathrm{Li}^+ + x\mathrm{e}^- \rightarrow \mathrm{Li}_x\mathrm{MFeO_4} \quad \mathrm{M} = \mathrm{K_2}, \mathrm{Ba}, \mathrm{Li_2}, \text{etc.} \tag{11}$$

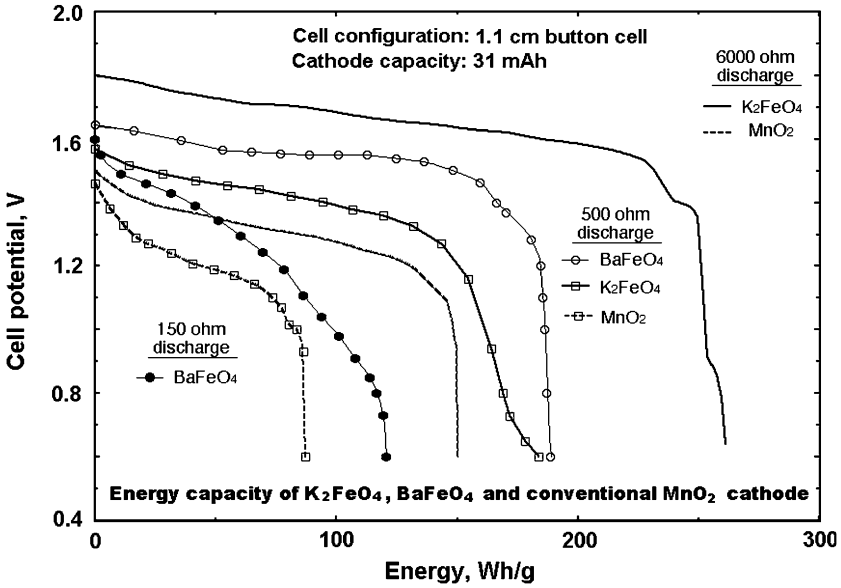

Fig. 11 Energy capacity comparison of K_2FeO_4, $BaFeO_4$, and conventional MnO_2 cathodes (with a Zn anode) [7]

Figure 16 compares the nonaqueous discharge of Li_2FeO_4, K_2FeO_4, and $BaFeO_4$ cathode batteries with a LiTFB PC:DME (lithium tetrafluoroborate dissolved in propylene carbonate/dimethoxyethane) electrolyte and a lithium anode. Under the same condition, the $BaFeO_4$ cathode exhibits lower polarization losses and higher discharge efficiency than the K_2FeO_4 cathode. However, due to its lighter mass, the observed capacity of the K_2FeO_4 is marginally higher. Li_2FeO_4 exhibits a high capacity in the nonaqueous discharge, approaching 600 mAh/g [11].

Syntheses of $KMnO_4$-, ZrO_2-, TiO_2-, and SiO_2-coated Fe(VI) cathodes

Generally, the less soluble $BaFeO_4$ salt is expected to be more stable than K_2FeO_4, but the chemically synthesized $BaFeO_4$ is somewhat less stable [21, 28]. Licht et al. found that 5% $KMnO_4$ coating was able to improve the $BaFeO_4$ robustness [9]. Specially, the coating can be prepared through an organic medium (e.g., acetonitrile) with $KMnO_4$ as the coating material. The $KMnO_4$ can be dissolved in

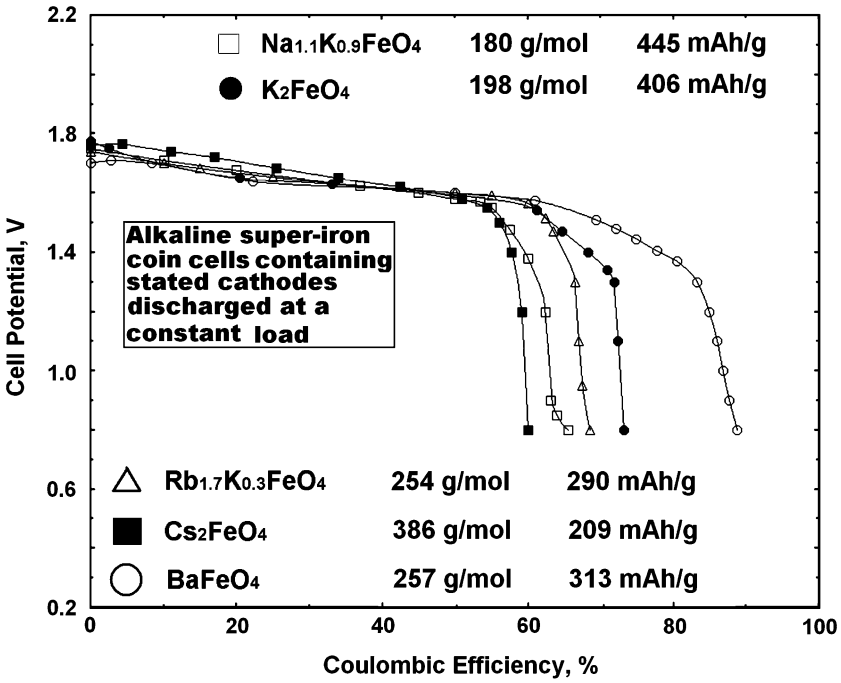

Fig. 12 Alkaline Fe(VI) coin cells (zinc anode) containing either a $BaFeO_4$, Cs_2FeO_4, K_2FeO_4, $Rb_{1.7}K_{0.3}FeO_4$, or $Na_{1.1}K_{0.9}FeO_4$ cathode discharged at a constant load of 3,000 Ω [30]

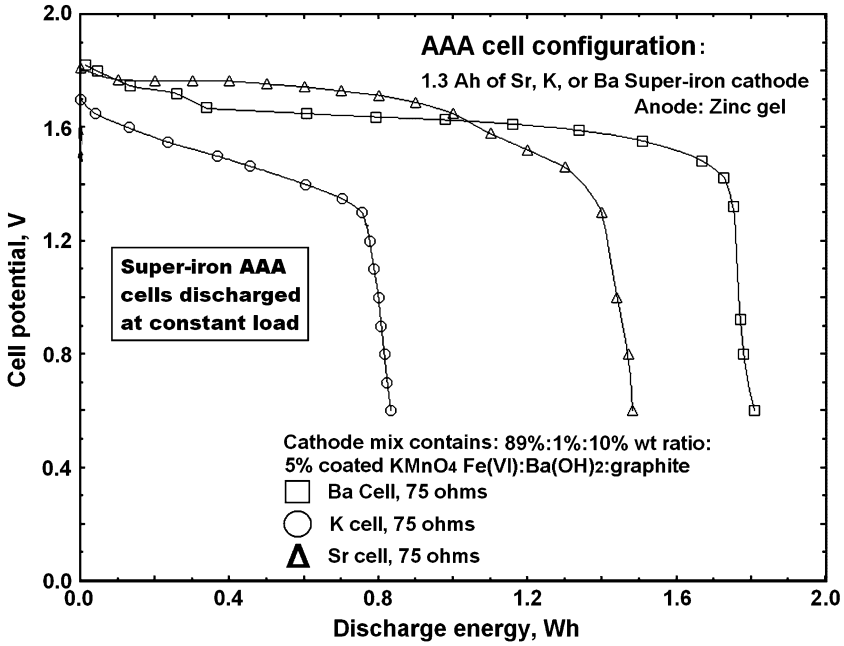

Fig. 13 Alkaline Fe(VI) AAA (44.5 mm long and 10.5 mm in diameter, cylindrical battery) cells containing either a K_2FeO_4, $BaFeO_4$, or $SrFeO_4$ discharged at constant load [12]

acetonitrile, but the $BaFeO_4$ is insoluble in this solution. Therefore, in the $KMnO_4$-dissolved acetonitrile media, upon sufficient stirring and removal of organic solvent, the solid $BaFeO_4$ powder is coated with $KMnO_4$ [9].

Among the Fe(VI) cathodes, K_2FeO_4 exhibits higher solid-state stability and higher intrinsic $3e^-$ capacity. At low current densities, the K_2FeO_4 cathode can approach the intrinsic (406 mAh/g) storage capacity [7]. However, the discharge of Fe(VI) forms a ferric overlayer [29, 38]; upon storage, the bulk Fe(VI) remains active but the overlayer passivates the Fe(VI) cathode towards further discharge. Therefore, whereas the fresh pure K_2FeO_4 discharges well, the capacity of K_2FeO_4 decreases seriously after storage [39]. Licht's group developed a novel zirconia coating methodology, and only 1% zirconia coating can dramatically improve the capacity of K_2FeO_4 after storage [39].

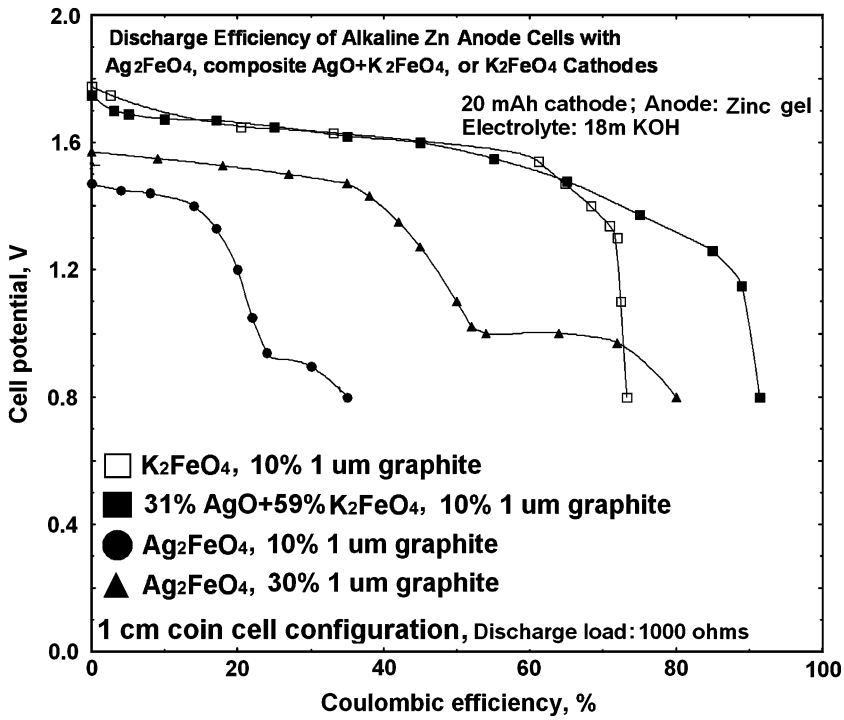

Fig. 14 Alkaline Zn anode Fe (VI) cells containing either Ag_2FeO_4, AgO/K_2FeO_4 composite, or only K_2FeO_4 as a cathode discharged at a constant load of 1,000 Ω [33]

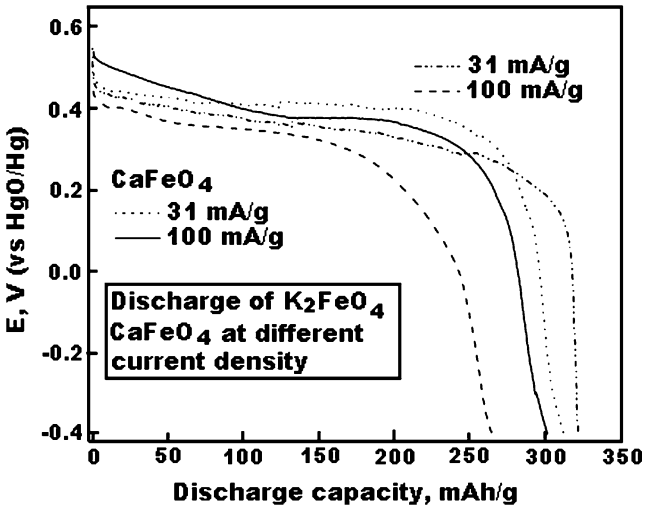

Fig. 15 Discharge of $CaFeO_4$ and K_2FeO_4 cathodes at 15 °C at indicated discharge current density [47]

The novel zirconia coating can be derived from an organic (ether) soluble zirconium salt (e.g., $ZrCl_4$). A 1 wt% zirconia coating, prepared with 30 min coating time, has been observed to have the best effect on charge retention of a coated cathode. This ZrO_2 methodology is also available for coating other Fe(VI) cathodes, such as Cs_2FeO_4 and $BaFeO_4$ [45]. Attenuated total reflectance Fourier transform infrared (ATR/FTIR) spectrometry analysis results of several uncoated and coated Fe(VI) cathodes are illustrated in Fig. 17. Spectrum of the pure ZrO_2 is also shown here for comparison. The 1,396 and 1,548 cm^{-1} peaks on the coated material is proved to be consistent with the FTIR spectra of pure $ZrO_2/Zr(OH)_4$ depending on extent of hydration [71]:

$$ZrCl_4 + 2O_2 \rightarrow ZrO_2 + 2Cl_2; \qquad ZrO_2 + 2H_2O \leftrightarrow Zr(OH)_4 \tag{12}$$

Stabilized zirconia has been introduced as a pH sensor for high temperature aqueous systems, [72] and $Zr(OH)_4$ has long been known as a hydroxide ion conductor which will readily exchange between solution phase hydroxide, phosphate, fluoride, and sulfate [73–76]. Licht et al. proposed the protection mechanism of the zirconia coating that: the insoluble Zr centers provide an intact shield, as represented in Fig. 18, and with Eq. 12, a hydroxide shuttle is necessary to sustain alkaline cathode redox chemistry [39, 45]. Solid stable Fe(VI) cathodes, K2FeO4 and Cs2FeO4, are effectively protected by the presence of this zirconia overlayer from the passivation in alkaline electrolyte. However, only a little stabilization effect is observed for the chemical decomposition of solid-state unstable cathode BaFeO4 [45].

SiO_2 and TiO_2 coatings for Fe(VI) salts were first reported by Walz et al. [40, 46]. In their studies, silicon dioxide and titanium dioxide thin film coatings were applied to $BaFeO_4$ by an aqueous sol–gel technique. Figure 19 illustrates the long-term stability of dry nanoporous silica-coated $BaFeO_4$ compared with uncoated $BaFeO_4$. As seen in the figure, the silica-coated $BaFeO_4$ showed a significant improvement in stability, maintaining nearly 80% of the Fe(VI) activity for 40 weeks [40]. TiO_2-coated Fe(VI) does not demonstrate

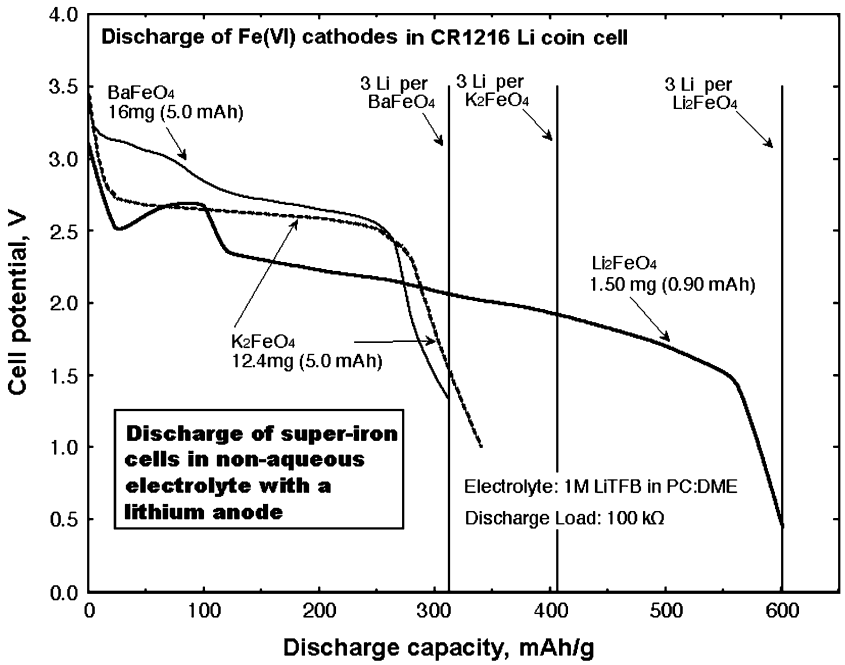

Fig. 16 Constant load discharge of cells containing a Li_2FeO_4, K_2FeO_4, or $BaFeO_4$ Fe(VI) cathode and a lithium anode. Electrolyte is 1 M LiTFB PC:DME (1 M lithium tetrafluoroborate dissolved in propylene carbonate/dimethoxyethane) [11]

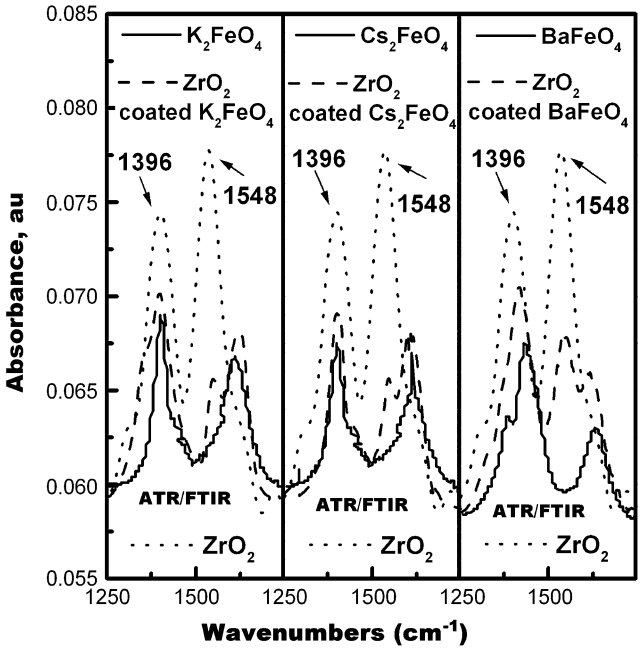

Fig. 17 IR absorption spectra of ZrO_2-coated and uncoated cathode materials K_2FeO_4, Cs_2FeO_4 and $BaFeO_4$. Spectra are obtained by attenuated total reflectance Fourier transform infrared (ATR/FT-IR) spectrometry. Spectra of 5% coating included for emphasis [45]

good shelf life in alkaline electrolyte, but provides more favorable results in the nonaqueous lithium cells [46].

Preparation of reversible Fe(III/VI) thin films

Whereas primary Fe(VI) charge transfer had been extensively demonstrated, reversible charge transfer of Fe(VI) cathodes had always been problematic. In principle, a sufficiently thin Fe(VI) cathode should facilitate electronic communication with a conductive substrate to sustain cycled charge storage. However, a variety of Fe(VI) thin cathodes, formed by pressure and/or mix with a granular conductor such as small particle carbons, [26] had passivated upon charge/discharge cyclings. In 2004, Licht's group first observed that rechargeable Fe(VI/III) films can be generated, by electro-deposition onto conductive substrates from solution phase Fe(VI) electrolytes [29]. In this

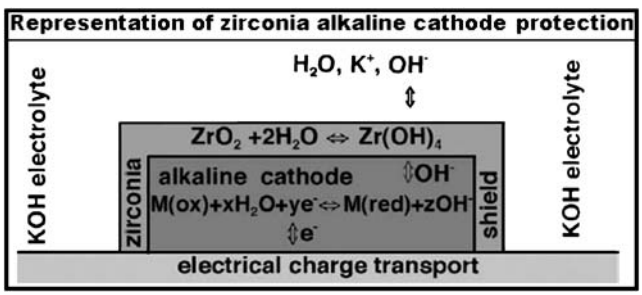

Fig. 18 Representation of zirconia alkaline cathode protection [39]

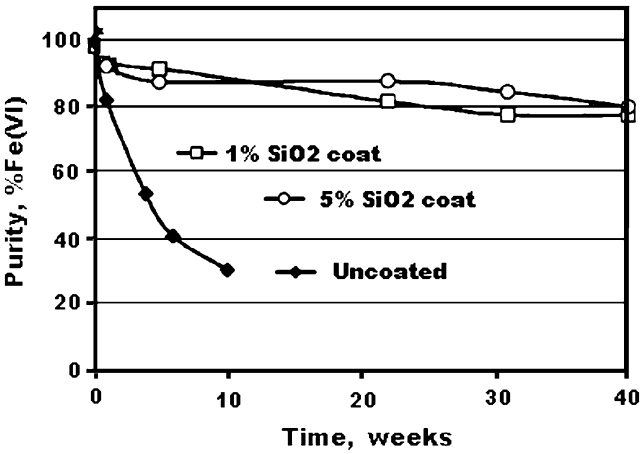

Fig. 19 Long-term stability of coated $BaFeO_4$ compared with uncoated reference [40]

study, a nanofilm (3 nm) was generated on a smooth Pt foil electrode from micro-pipette controlled, microliter volumes of dissolved Fe(VI) in alkaline solution, by applying a certain potential (100 mV vs. Ag/AgCl) to the Pt foil substrate. This film was rigorous and highly reversible when used as a storage cathode. As demonstrated as an example in Fig. 20, an 80% DOD (depth of discharge) of the 485 mAh/g capacity Na_2FeO_4 film can be maintained after 100 galvanostatic cycles [29].

Whereas ultra-thin Fe(VI) films can sustain an extended reversibility, thicker films were not rechargeable due to the irreversible buildup of passivating (resistive) Fe(III) oxide, formed during film reduction. In 2006, Licht's group probed that preparation of Fe(III/VI) films on an extended conductive matrix can facilitate the thick film's reversibility [38]. In these studies, substrates for the film preparation were selected from Pt or Ti foils. The extended conductive matrixes were prepared through electrochemically depositing platinum or Pt–Au codeposition on the substrates. Fe(VI) films were electrodeposited from K_2FeO_4 as dissolved in NaOH solution onto the extended substrates. The mechanism of the Fe(VI) film deposition is not yet very clear so far. Generally, the Fe (VI) was considered to be converted to Fe(III) by a electrochemical process during the film formation [29, 38].

With the extended conductive matrix as the film substrate, a substantial improvement to sustain thick Fe (VI) film charge transfer is obtained. Specially, in a half-cell configuration, a 100-nm Fe(VI) cathode, electrodeposited on the extended conductive matrixes, sustained 100–200 reversible three-electrode galvanostatic charge/discharge cycles, and a 19-nm thin film cathode sustained 500 such cycles. In a full cell (in conjunction with a metal hydride anode), a 250-nm Fe(VI) film sustained 40 charge/discharge cycles, and a 25-nm film was reversible throughout 300 cycles [38]. Using Ti foil as the substrate, a 50-nm Fe(III) film on platinized Ti can sustain over 200 charge/discharge cycles. When Pt–Au codeposited Ti surface was

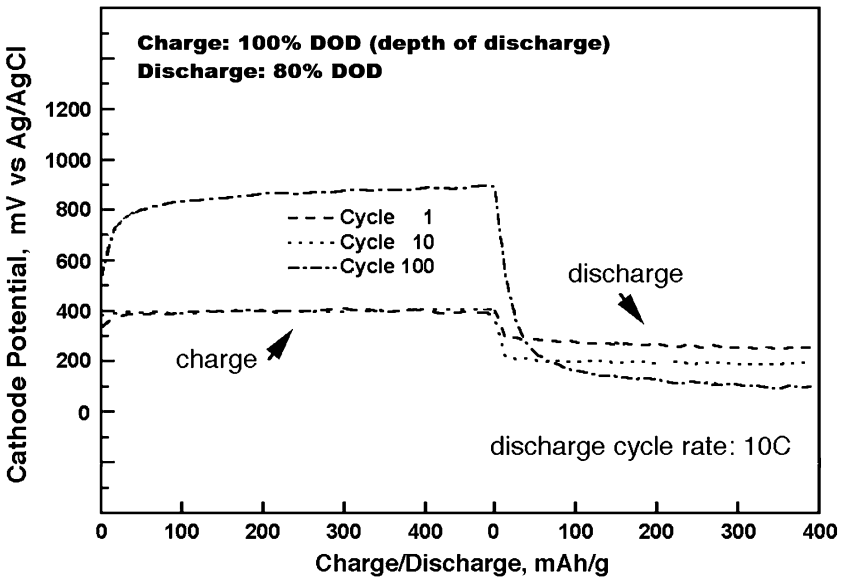

Fig. 20 Reversible charge storage of a Fe(VI) of a 485 mAh/g capacity Na_2FeO_4 nanofilm in alkaline electrolyte (10 M NaOH). The nanofilm (~3 nm) was formed by potentiostatic reduction of 0.38 μl 5 mM Na_2FeO_4 dissolved in 10 M NaOH onto 0.3 cm^2 Pt foil [29]

used as the substrate. A 300-nm Fe(VI) film displayed a moderate charge/discharge cycle life of 20 [38].

The facilitated Fe(VI) charge transfer, upon charge/discharge, as a result of the expanded conductive matrix to facilitate charge transfer, is demonstrated in Fig. 21. Without direct contact with the substrate, the Fe(III) centers (shaded) in Fig. 21a had posed an impediment to charge transfer. This could be partially (Fig. 21b) and fully alleviated (Fig. 21c) by intimate contact with the enhanced conductive matrix, which maintains extended direct contact with the substrate [29, 38].

Thin Fe(VI/III) films also exhibit extensive, high-capacity nonaqueous rechargeability. Reversibility of the electrodes has been probed using thin films of K_2FeO_4 on Pt foils in a PC/DME 2:1 1 M $LiClO_4$ electrolyte (Fig. 22) [37]. As seen in Fig. 22, K_2FeO_4 thin-film electrodes could be cycled reversibly at a capacity above 300 mAh g^{-1} with a little capacity fading during prolonged cycling.

Fe(VI) analysis

This section focuses on the analysis of synthesized Fe(VI) compounds. Analytical Fe(VI) methodologies summarized are FTIR spectroscopy, titrimetric (chromite), UV/Vis spectroscopy, XRD, ICP spectroscopy, Mössbauer spectroscopy, potentiometric, galvanostatic, and cyclic voltammetry.

FTIR Fe(VI) analysis

The FTIR spectroscopy can be used as a quantitative tool for the determination of Fe(VI) compounds. However, the small sample size, comprising only ~1% by weight of the KBr pellet, as well as the precise placement of the pellet in the spectrometer, provides challenges to the quantitative analysis of the spectra. These challenges can be overcome by the use of an added standard, added as a fixed concentration to the sample, prior to extracting a segment of the sample to prepare the KBr pellet [14, 47]. The Fe(VI) FTIR standard should have the favorable characteristics: (1) that it is inert towards Fe(VI) compounds and (2) with a clear, intrinsic IR spectra isolated from the Fe(VI) absorption bands [14, 30, 32, 40, 47]. In Licht's study, the Fe(VI) standard is provided by addition of $BaSO_4$, which provides a reproducible, inert, and distinctive, but isolated, IR absorption. In this procedure for quantitative Fe(VI) analysis, detailed in the work of Licht et al. [14], a KBr pellet is formed which contains a known mass of $BaSO_4$, as well as a known mass of the sample to be analyzed, and the FTIR spectrum measured. As seen in Fig. 23 and in the figure insert, the absorbance of $BaFeO_4$ at 780 cm^{-1} relative to the $BaSO_4$ absorbance at 1,079 cm^{-1} (or 1,183), of a fixed concentration or $BaSO_4$, grows in linear proportion to the $BaFeO_4$ concentration and provides a route for quantitative analysis of the $BaFeO_4$ concentration. The analysis utilizes k, the $BaSO_4$ to $BaFeO_4$ conversion constant, defined by the absorptivity of $BaSO_4$ compared to that of $BaFeO_4$, in a standard sample containing equal $BaSO_4$ and $BaFeO_4$ weight fractions:

$$k(\text{wt\% BaFeO}_4 = \text{wt\% BaSO}_4) \equiv A_{\text{BaSO}_4}\left(1,079\text{cm}^{-1}\right)/A_{\text{BaFeO}_4}\left(780\text{cm}^{-1}\right) \quad (13)$$

ICP Fe(VI) analysis

Inductively coupled plasma analysis of K_2FeO_4 and $BaFeO_4$ samples has been reported (conducted with an

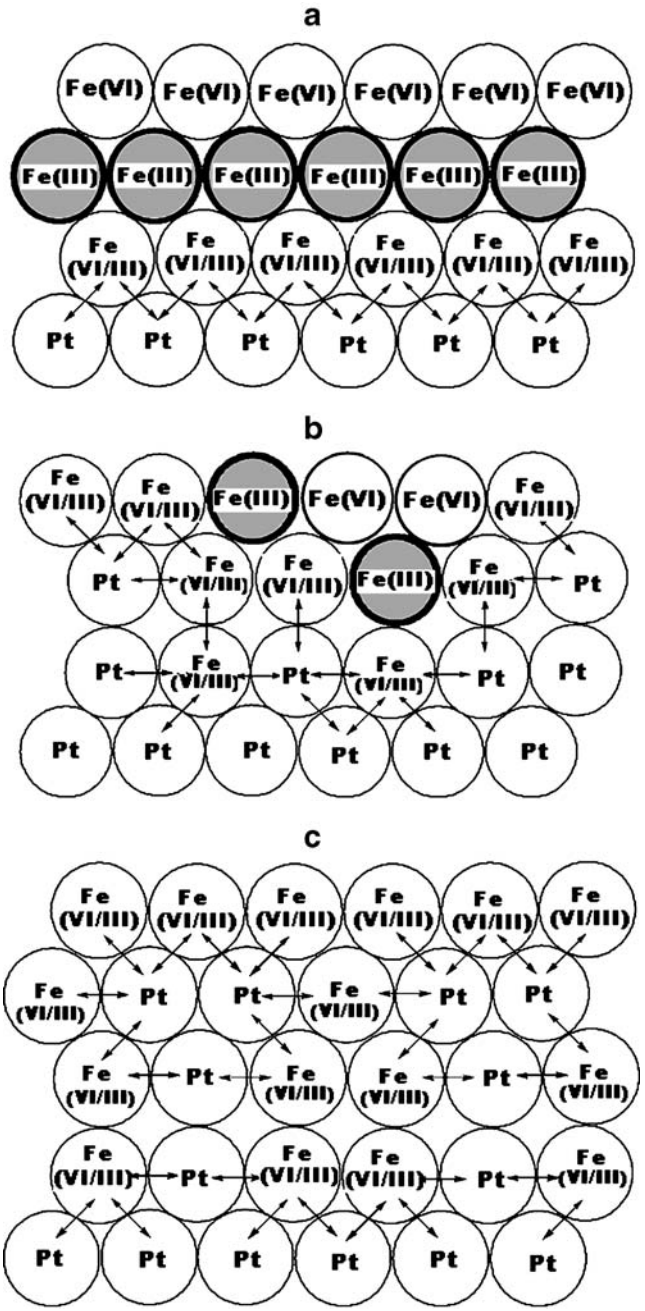

Fig. 21 Representation of Fe(III/VI) passivation (**a**), as well as the partial (**b**) and full (**c**) alleviation through an extended conductive matrix in Fe(III/VI) ferrate films [38]

ICP Perkin-Elmer Optima 3000 DV) to determine the relative weight percent and mole percent compositions of the principal cations and possible impurities in the sample [14]. Such conventional ICP analytical methodologies provide elemental composition information but not information regarding a compound's valence state. Hence, these methodologies are convenient, but not specific, to Fe(VI) analysis and are only briefly described in this section. These methodologies, or related atomic absorption or emission and X-ray fluorescence techniques, are important to determine total iron relative to other elements in a Fe(VI) compound. From these values, the mole ratio of principal cations, the mass percent of the principal cations, and the maximum contribution of alternate cation impurities is determined [14].

Titrimetric (chromite) Fe(VI) analysis

Following the quantitative determination of total iron in a compound, for example as described by ICP analysis, the extent of the iron existing in the Fe(VI) valence state can be determined by titrimetric chromite analysis. Alternately, if the type of Fe(VI) compound is known (for example as K_2FeO_4 or $BaFeO_4$), then the sample's mass yields the theoretical oxidation capacity (calculated as three equivalents per Fe), which in turn is compared with the chromite analyzed oxidation capacity.

The chromite analysis methodology varies with the specific Fe(VI) compound to be ascertained [14]. For example, the highly insoluble $BaFeO_4$ compound must be heated during dissolution, and alternate competing oxidants must be removed. In each case, the Fe(VI) sample is dissolved into solution as FeO_4^{2-} to oxidize chromite, Cr (III) to chromate Cr(VI):

$$Cr(OH)_4^- + FeO_4^{2-} + 3H_2O \rightarrow Fe(OH)_3(H_2O)_3 + CrO_4^{2-} + OH^- \quad (14)$$

The generated chromate is then titrated with a standard ferrous ammonium sulfate solution, using an aqueous sodium diphenylamine sulfonate indicator solution.

UV/Vis Fe(VI) analysis

Fe(VI), dissolved as FeO_4^{2-}, has a distinctive UV/Vis spectrum. However, the quantitative analysis of solid Fe (VI) salts by dissolution and UV/Vis absorption spectroscopy is limited by the relative insolubility of Fe(VI) salts such as $BaFeO_4$ in aqueous solutions [8], the general tendency of Fe(VI) salt insolubility in a wide variety of organic solvents [11], and the tendency of dissolved aqueous Fe(VI) salts to decompose in aqueous solutions other than specific electrolytes, such as highly concentrated KOH electrolytes, and electrolytes specifically excluding Ni(II) and Co(II) catalysts [7, 77]. The decomposition with water takes the form of Eq. 6. When occurring, the decomposition tends to lead to the formation of colloidal ferric(III) oxide and to limit the time available for Fe(VI) analysis. Colloidal ferric oxide interference is minimized by a 385-nm baseline correction and/or solution centrifugation prior to spectroscopic analysis. The visible absorption spectrum of Fe(VI) in highly alkaline solution exhibits a maximum at 505 nm, an absorption shoulder at 570 nm and

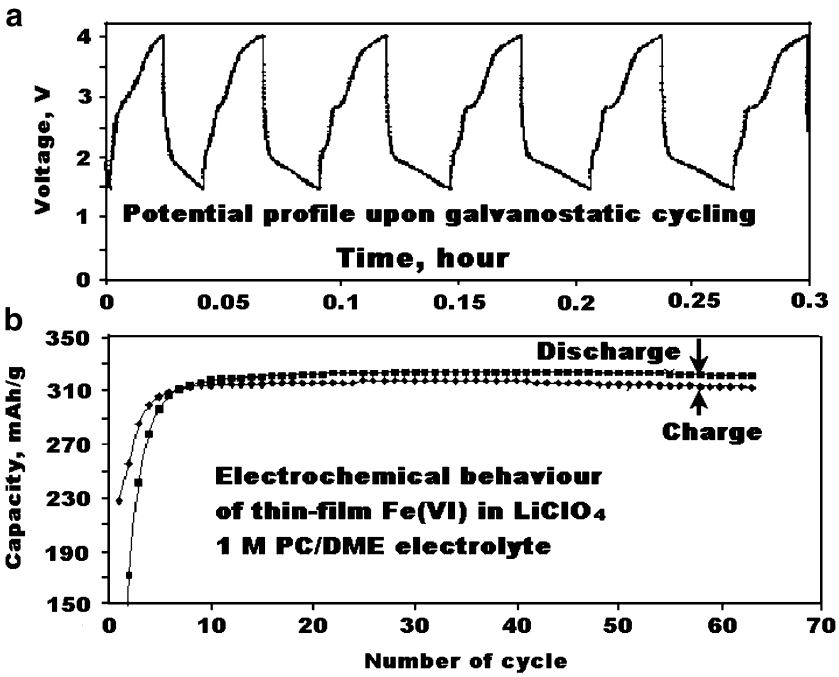

Fig. 22 The electrochemical behavior of a thin film K_2FeO_4 on a Pt electrode. The thin film is cycled in a $LiClO_4$ 1 M PC/DME 2:1 solution: (**a**) typical potential profile of these electrodes upon galvanostatic cycling and (**b**) charge and discharge capacity vs. cycle number (galvanostatic cycling at *C*/10 rates) [37]

two minima at 390 and 675 nm. The molar absorptivity measured at 505 nm is 1,070±30 M^{-1} cm^{-1}. The molar absorptivity remained constant up to 200 mM. Similarly, at a fixed ferrate concentration, the measured absorbance was independent of alkali hydroxide cation and concentration [14]. Hence, to within better than 5%, the 505 nm absorbance of 2 mM K_2FeO_4 is the same in 5 M Li, Na, K, and Cs hydroxides and also the same in 5–15 M NaOH, 5–13.5 M KOH, and 5–15 M CsOH [14].

XRD Fe(VI) analysis

The measured powder X-ray diffraction spectra of Fe(VI) compounds exhibit little variation using salts ranging averaging in particle size from 35 to 100 μm, or measured with a wide range of (2) scan rates. The obtained XRD spectra are often consistent with an orthorhombic crystal system with the spaces group D_{2h} (Pnma) [14, 29, 32, 40, 47]. Although often used as a tool for qualitative rather than

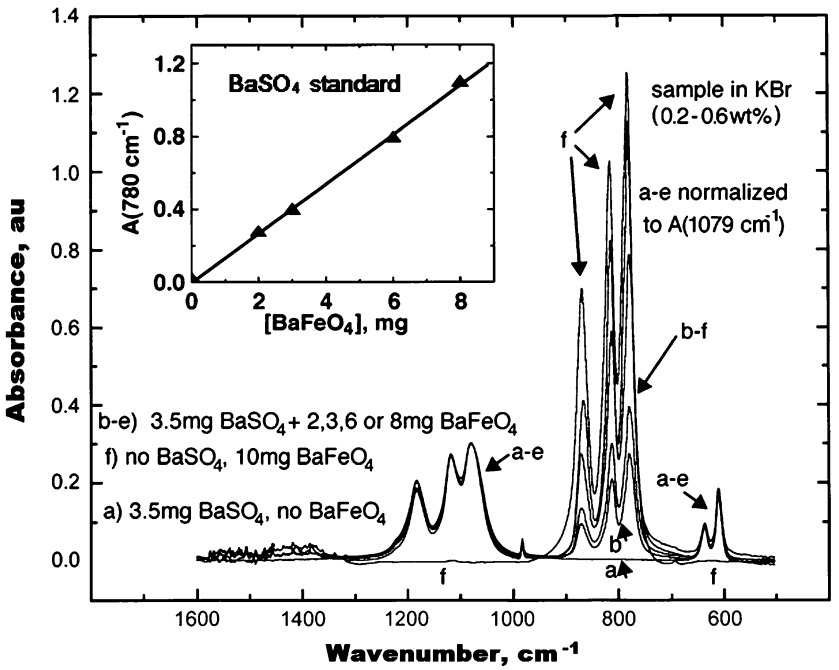

Fig. 23 FTIR analysis of $BaFeO_4$ utilizing a $BaSO_4$ standard [14]

quantitative analysis, XRD was also used to distinguish between coated barium ferrate from pure barium ferrate [14, 30]. For example, a several percent coating from $KMnO_4$ is distinguishable as a low level of the expected, known $KMnO_4$ XRD pattern superimposed on the regular $BaFeO_4$ pattern. Graphite and carbon blacks added to an Fe(VI) mix in the preparation of a cathode do not significantly interfere with the observed Fe(VI) XRD patterns [14].

Fe(VI) Mössbauer analysis

Mössbauer analysis is an excellent means to distinguish the valent states of iron [26, 37, 78–81]. In recently reports [26, 37], ex situ Mössbauer spectroscopy and in situ electrochemical Mössbauer spectroscopy Fe(VI) studies were performed using a conventional constant acceleration Mössbauer drive and a 50 mCi^{57} Co:Rh source. The velocity calibration and isomer shift reference are those of a thin foil of α-iron. For the quantitative Fe(VI) or Fe(III) analysis, The spectra were analyzed by a least-squares fit program to several quadrupole doublets. The relative areas of the doublets were taken as the relative abundances of the Fe(VI) and Fe(III) components [37]. Figure 24 compares the Mössbauer spectra of a sample containing pure K_2FO_4 and a sample that K_2FO_4 has been partially reduced to the Fe(III) valence state [37]. Combined with the electrochemical techniques, the in situ Mössbauer spectroscopy would be an useful tool for the mechanism study of the Fe(VI) charge/discharge behavior.

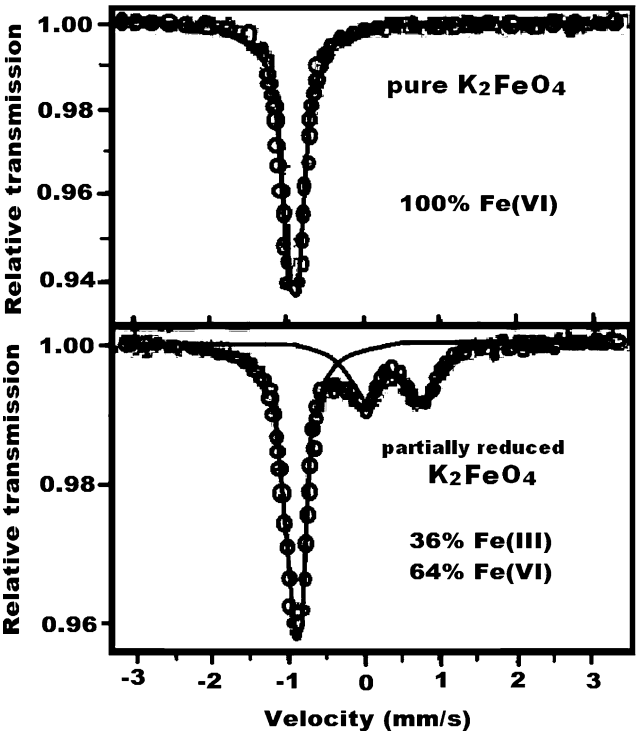

Fig. 24 Mössbauer spectra of a sample containing pure K_2FeO_4 (Fe (VI) or K_2FO_4 partially reduced to the Fe(III) valence state [37]

Fe(VI) electrochemical analyses

Electroanalytical techniques to probe Fe(VI) compounds can be conveniently categorized as either solution phase (dissolved Fe(VI)) or solid cathode techniques. Solution electrochemical techniques such as potentiometric, galvanostatic, and cyclic-voltammetry methods are convenient, and can be carried out using a conventional potentiostat in a three-electrode electrochemical cell. Fe(VI) electrochemical analyses summarized here include:

(1) Fe(VI) potentiometric analysis: The measured redox potentials, at platinum electrode, of K_2FeO_4 in various NaOH solutions was measured yielding $E^{\circ}(\text{inNaOH})_{FeO_4^{2-}} = 0.66 \pm 0.01\text{V}$ (SHE). As expected, redox potential shifts to more positive values with log of the increase in ferrate concentration and was analyzed in detail in the work of Licht et al. [14]. In aqueous alkali and alkali earth hydroxide electrolytes, a variety of Fe (VI) compounds, over a wide concentration range, exhibit a potential varying from 0.55 to 0.75 V vs. SHE [14].

(2) Fe(VI) solution phase galvanostatic analysis [14]: Galvanostatic reduction of dissolved ferrate yields a direct electrochemical measurement of the oxidation state of iron in ferrate. Figure 25 presents the time evolution of the potential during ferrate reduction. A $c_{initial}$=2 mM potassium ferrate solution in v=3 ml of 15 M NaOH is reduced at a current density J=10 μA/cm^2. Integration of the charge transferred yields the relative oxidation state, $\Delta q'$, where F is the Faraday constant and t is time:

$$\Delta q' = t \times J/(c_{initial} \times v \times F) \quad (15)$$

and which may be compared to the intrinsic charge of the insoluble Fe(III) product. A planar platinum electrode does not provide the optimum surface to probe solution phase Fe(VI) reduction. The Pt surface tends to passivate in time as the reduced Fe(III) layer builds on the surface. This passivation is alleviated by (1) minimizing the thickness of the layer, employing low volumes and low concentrations of dissolved Fe(VI) salts, (2) using low initial current densities, such as 10 μA cm^{-2}, and (3) further diminishing the current by an order of magnitude as the overpotential increases towards the end of the reduction. Under these conditions, and as seen in the curve in Fig. 25, the oxidation state of the starting material approaches Fe(VI).

(3) Fe(VI) cyclic voltammetry analysis: Representative voltammetric curves for the reduction of K_2FeO_4 dissolved in 15 M NaOH at a Pt electrode are shown in Fig. 26 and are further detailed in reference [14].

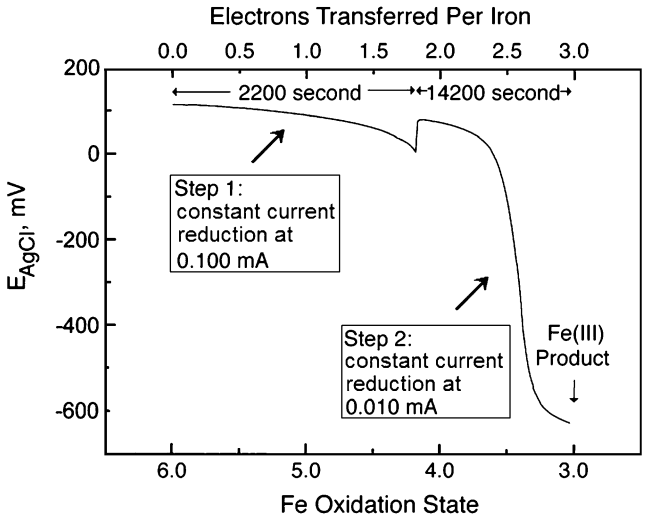

Fig. 25 Determination of the oxidation state of iron in ferrate(VI) solutions. Galvanostatic reduction of 2.5 mM K_2FeO_4 in 0.5 ml 13.5 M KOH solution. The electrode is 10 cm^2 Pt [14]

The negative potential scan reveals a cathodic current of ferrate(VI) reduction at potentials less positive than 200 mV, and cathodic reduction of ferrate(VI) proceeds with an overvoltage of approximately 150 mV. O_2 evolution in the oxidation sweep interferes with oxidation of ferrate(III). The peak cathodic current density increased linearly with ferrate concentration and was proportional to (scan rate)$^{1/2}$, indicating diffusion limitation of ferrate(VI) reduction.

Summaries

In this review, two Fe(VI) synthetic routes including the solution phase synthesis and solid-state synthesis are summarized. Fe(VI) compounds with synthetic details summarized in this paper are the alkali Fe(VI) salts Li_2FeO_4, $K_xNa_{(2-x)}FeO_4$, K_2FeO_4, Rb_2FeO_4, Cs_2FeO_4, as well as alkali earth Fe(VI) salts $BaFeO_4$, $SrFeO_4$, $CaFeO_4$, and a transition metal Fe(VI) salt Ag_2FeO_4. Alkaline and nonaqueous discharge of the synthesized Fe(VI) cathodes are presented. Fe(VI) salts are capable of efficient three-electron (for Ag_2FeO_4, five-electron) reduction and sustain high electrochemical storage capacity.

Preparation of thin-film reversible Fe(VI/III) cathodes are summarized in this paper. Highly reversible Fe(III/VI) films can be electrochemically deposited on either smooth conductive substrates or on extended conductive matrixes. Ultra-thin (3-nm) Fe(III/VI) films exhibited a high degree of three-electron reversibility, However, thicker films had been increasingly passive toward the Fe(VI) charge transfer. Extended conductive matrix facilitates a two orders of magnitude enhancement in charge storage for reversible Fe (III/VI) thin films.

A low level (1%) zirconia coating derived from $ZrCl_4$ through organic medium can significantly stabilize the high capacity Fe(VI) cathode and enhanced the stability and electrochemical capacity of Fe(VI) batteries. A 5% $KMnO_4$ coating prepared through acetonitrile solvent can improve the robustness of chemical synthesized $BaFeO_4$. The silica-coated Fe(VI) salts showed a significant improvement in

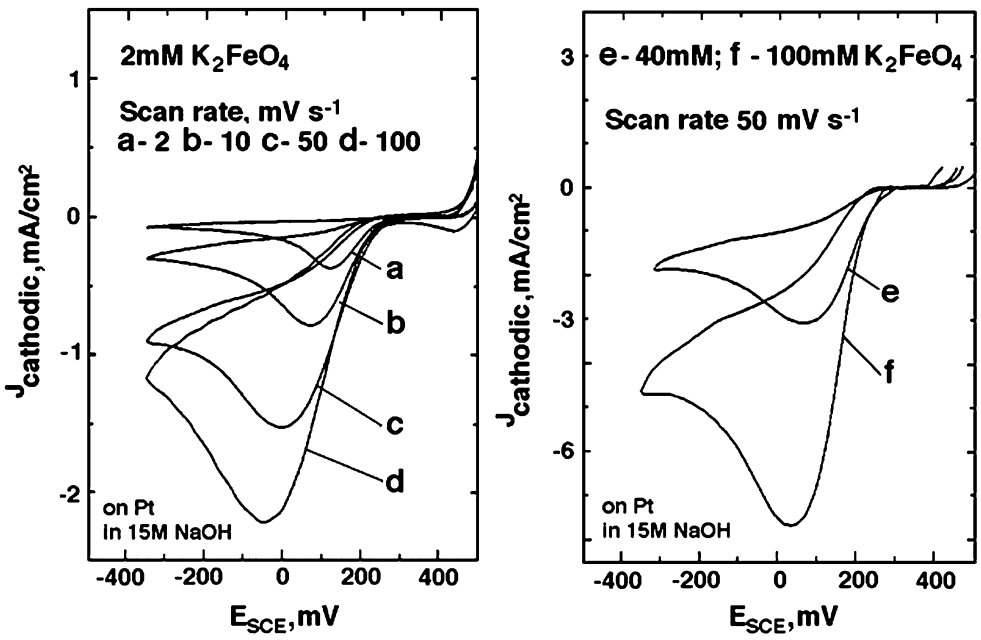

Fig. 26 Cyclic voltammetry of ferrate(VI) solutions. *Left* variation with potential scan rate; *right* variation with ferrate(VI) concentration [14]

stability. TiO_2-coated Fe(VI) materials demonstrated poor shelf life in alkaline electrolyte, but provided somewhat more favorable results in the lithium cells.

Analysis of Fe(VI) is an important aspect in Fe(VI) studies. Various Fe(VI) analytical methodologies including FTIR spectroscopy, titrimetric (chromite), UV/Vis spectroscopy, XRD, ICP spectroscopy, Mössbauer spectroscopy, potentiometric, galvanostatic, and cyclic voltammetry are summarized in this paper.

References

1. Carr JD, Kelter PB, Tabatabai A, Splichal D, Erickson J, Mclaughlin CW (1985) In: Jolly RL (ed) Proc. 5th Conference of Water Chlorination. Lewis, Chelsea, MI, pp 1285
2. Sharma VK, Smith JO, Millero FJ (1997) Environ Sci Technol 31:2486
3. Licht S, Yu X (2005) Environ Sci Technol 39:8071
4. Jiang JQ (2007) J Hazard Mater 146:617
5. Jiang J, Wang S, Panagoulopoulos A (2007) Desalination 210:266
6. Delaude L, Laszlo P (1996) J Org Chem 61:6360
7. Licht S, Wang B, Ghosh S (1999) Science 285:1039
8. Licht S, Wang B, Ghosh S, Li J, Naschitz V (1999) Electrochem Commun 1:522
9. Licht S, Wang B, Xu G, Li J, Naschitz V (1999) Electrochem Commun 1:527
10. Licht S, Wang B, Li J, Ghosh S, Tel-Vered R (2000) Electrochem Commun 2:535
11. Licht S, Wang B (2000) Electrochem Solid-State Lett 3:209
12. Licht S, Naschitz V, Ghosh S, Lin L, Liu B (2001) Electrochem Commun 3:340
13. Licht S, Naschitz V, Ghosh S, Liu B, Halperine N, Halperin L, Rozen D (2001) J Power Sources 99:7
14. Licht S, Naschitz V, Lin L, Chen J, Ghosh S, Liu B (2001) J Power Sources 101:167
15. Licht S, Ghosh S, Dong Q (2001) J Electrochem Soc 148:A1072
16. Licht S, Naschitz V, Ghosh S (2001) Electrochem Solid-State Lett 4:A209
17. Licht S, Ghosh S, Naschitz V, Halperin N, Halperin L (2001) J Phys Chem B 105:11933
18. Licht S, Ghosh S (2002) J Power Sources 109/2:465
19. Licht S, Naschitz V, Ghosh S (2002) J Phys Chem B 106:5947
20. Licht S, Tel-Vered R, Halperin L (2002) Electrochem Comm 4:933
21. Licht S, Naschitz V, Wang B (2002) J Power Sources 109:67
22. Lee J, Tryk D, Fujishima A, Park S (2002) Chem Commun 5:486
23. Yang W, Wang J, Pan T, Xu J, Zhang J, Cao C (2002) Electrochem Commun 4:710
24. Yang W, Wang J, Zhang Z, Zhang J, Cao C (2002) Chin Chem Lett 13:761
25. Tel-Vered R, Rozen D, Licht S (2003) J Electrochem Soc 150: A1671
26. Ghosh S, Wen W, Urian RC, Heath C, Srinivasamurthi V, Reiff W, Mukerjee S, Naschitz V, Licht S (2003) Electrochem Solid-State Lett 6:A260
27. De Koninck M, Brousse T, Belanger D (2003) Electrochim Acta 48:1425
28. Licht S, Tel-Vered R, Halperin L (2004) J Electrochem Soc 151: A31
29. Licht S, Tel-Vered R (2004) Chem Commun 6:628
30. Licht S, Naschitz V, Rozen D, Halperin N (2004) J Electrochem Soc 151:A1147
31. Zhang C, Liu Z, Wu F, Lin L, Qi F (2004) Electrochem Commun 6:1104
32. Walz K, Suyama A, Suyama W, Sene J, Zeltner W, Armacanqui E, Roszkowski A, Anderson M (2004) J Power Sources 134:318
33. Licht S, Yang L, Wang B (2005) Electrochem Commun 7:931
34. Nowik I, Herber RH, Koltypin M, Aurbach D, Licht S (2005) J Phys Chem Solids 66:1307
35. Koltypin M, Licht S, Tel-Vered R, Naschitz V, Aurbach D (2005) J Power Sources 146:723
36. Ayers K, White N (2005) J Electrochem Soc 152:A467
37. Koltypin M, Licht S, Nowik I, levi E, Gofer Y, Aurbach D (2006) J Electrochem Soc 153:A32
38. Licht S, DeAlwis C (2006) J Phys Chem B 110:12394
39. Licht S, Yu X, Zheng D (2006) Chem Commun 41:4341
40. Walz K, Szczech J, Suyama A, Suyama W, Stoiber L, Zeltner W, Armacanqui E, Anderson M (2006) J Electrochem Soc 153:A1102
41. Licht S, Yu X, Qu D (2007) Chem Commun 26:2753
42. Yu X, Licht S (2007) J Power Sources 171:966
43. Yu X, Licht S (2007) J Power Sources 171:1010
44. Yu X, Licht S (2007) Electrochim Acta 52:8138
45. Yu X, Licht S (2007) J Power Sources 173:1012
46. Walz K, Handrick A, Szczech J, Stoiber L, Suyama A, Suyama W, Zeltner W, Johnson C, Anderson M (2007) J Power Sources 167:545
47. Xu Z, Wang J, Shao H, Tang Z, Zhang J (2007) Electrochem Commun 9:371
48. Schryer J, Thompson G, Ockerman L (1951) J Am Chem Soc 73:1379
49. Li C, Li X, Graham N (2005) Chemosphere 61:537
50. Kanari N, Ostrosi E, Ninane L, Neveux N, Evrard O (2005) JOM 57:39
51. Wang Y, Zhou N, Ye S, Gao X (2003) Chin Electrochem 9:15
52. Bouzek K, Lipovska M, Schmidt M, Rousar I, Wragg A (1998) Electrochim Acta 44:547
53. De Koninck M, Belanger D (2003) Electrochim Acta 48:1435
54. He W, Wang J, Yang C, Zhang J (2006) Electrochim Acta 51:1967
55. Lapicque F, Valentin G (2002) Electrochem Commun 4:764
56. He W, Wang J, Shao H, Zhang J Cao C (2005) Electrochem Commun 7:607
57. Gump J, Wagner W (1954) Trans Kent Acad Sci 15:112
58. Gump J, Wagner W, Schreyer J (1954) Anal Chem 26:1957
59. Ettl V, Veprek-Siska J (1969) Collect Czechoslov Chem Commun 34:2182
60. Yang W, Wang J, Pan T, Cao F, Zhang J, Cao C (2004) Electrochim Acta 49:3455
61. Herber R, Johnson D (1979) Inorg Chem 18:2786
62. Losana L (1925) Gazzeta Chimica Italiana 55:468
63. Yang W, Wang J, Yang Z, Pan T, Zhang J (2005) Chin J Chem Phys 18:105
64. Firouzabadi H, Mohajer D, Moghaddam M (1986) Synth Commun 16:211
65. Wang Y, Muramatsu A, Sugimoto T (1998) Colloids Surf 134:281
66. Tripathi A, Kamble V, Gupta N (1999) J Catal 187:332
67. Audette R, Quail J (1972) Inorg Chem 11:1904
68. Sun Y, Pan J, Wan P, Liu X (2003) Chin J Power Sources 27:518
69. Lin Z, Chen Y, Chen R, Zheng X, Chen Z (2003) Chin Battery Bimonthly 33:187
70. Zhou Z, Liao Z (2003) Chin J Power Sources 27:497
71. Fang X, Fang C, Chen J (1996) J Chin Ceram Soc 6:732
72. Hettiarachchi S, Kedzierzawski P, Macdonald D (1985) J Electrochem Soc 132:1866
73. Chitrakar R, Tezuka S, Sonoda A, Sakane K, Ooi K, Hirotsu T (2006) J Colloid Interface Sci 297:426
74. Parks G, De Bruyn P (1962) J Phys Chem 66:967

75. King RB (1995) Ency Inorg Chem 8:4480
76. Clearfield A, Nancollas G, Blessing R (1973) In: Marinsky JA (ed) Ion exchange and solvent extraction, vol. 5. Decker, New York, pp 1–120
77. Jia H, Bao G (2004) Chin Battery Bimonthly 34:430
78. Jeannot C, Malaman B, GeHrardin R, Oulladiaf B (2002) J Solid State Chem 165:266
79. Deganelloa F, Liottaa L, Longoa A, Casalettoa M, Scopelliti M (2006) J Solid State Chem 179:3406
80. Dedushenko S, Zhizhin M, Perfiliev Y (2006) Hyperfine Interact 166:367
81. Tazi A, Bendriss A, Badrour L, Mouahid F, Zahir M (2005) Phys Chem News 26:104